

November 13, 2018

M SU-HEP-030701

BNL-NT-03/17

RBRC-329

Neutrino D meson Production and the Strangeness Asymmetry of the Nucleon

F. Olness^a, J. Pumplin^b, D. Stump^b, J. Huston^b, P. Nadolsky^a, H. L. Lai^c,
S. Kretzer^d, J. F. Owens^e, W. K. Tung^b

^aDepartment of Physics, Southern Methodist University

^bDepartment of Physics and Astronomy, Michigan State University

^cTaipei Municipal Teachers College, Taiwan

^dPhysics Department and RIKEN-BNL Research Center, Brookhaven National Laboratory

^eDepartment of Physics, Florida State University

We have performed the first global QCD analysis to include the CCFR and NuTeV dimuon data, which provide direct constraints on the strange and anti-strange parton distributions, $s(x)$ and $\bar{s}(x)$. To explore the strangeness sector, we adopt a general parametrization of the non-perturbative $s(x)$; $s(x)$ functions satisfying basic QCD requirements. We find that the strangeness asymmetry, as measured by the momentum integral $\int_0^1 x [s(x) - \bar{s}(x)] dx$, is sensitive to the dimuon data provided the theoretical QCD constraints are enforced. We study the range of uncertainty of $[s]$ using the Lagrange Multiplier method, which probes the quality of the global fit as a function of the strangeness parameters. Our estimate within the context of this global analysis is that $0.001 < [s] < 0.004$. Representative parton distribution sets spanning this range are given. Comparisons with previous work are discussed. These results contribute to the assessment of QCD corrections to the Paschos-Wolfeinstein relation, which is used in the measurement of the Weinberg parameter $\sin^2 w$ in N and \bar{N} scattering.

Contents

1	Introduction	2
2	General properties of $s(x)$ $s(x)$ and its first two moments	3
3	General parametrization of the strangeness distributions	5
4	Global Analysis	6
4.1	Procedure	8
4.2	Central Results	8
4.3	Range of $[S]$ by the Lagrange Multiplier Method	10
4.4	Additional Sources of Uncertainties	11
5	Comparisons to previous studies	13
6	Conclusion	14

1 Introduction

The recent measurements of both neutrino and antineutrino production of dimuon final states (charm signal) by the CCFR and NuTeV collaborations [1] provide the first promising direct experimental constraints on the strange and anti-strange quark distributions of the nucleon, $s(x)$ and $s(x)$. In addition to the intrinsic interest in nucleon structure, the strange asymmetry ($s - s$) has important implications on the precision measurement of the Weinberg angle in deep inelastic scattering of neutrinos.[2-6] We report here the first global QCD analysis that includes the new dimuon data, using the methods developed by the CTEQ collaboration, specifically to explore the strange and anti-strange parton parameter space.^a

In previous global analyses, information on s and s has resided only in inclusive cross sections for neutral and charged current DIS. The reliability of the extraction of the quite small s and s components^b (from differences of large cross sections measured in different experiments) was always in considerable doubt. For this reason, most global fits adopted the assumption $s(x) = s(x) = (u + d)/2$ (with 0.5) at some low value of Q^2 ; this approximation was inferred from the earlier combined neutrino and antineutrino dimuon experiments. The recent high-statistics dimuon measurements of [1] provide greater accuracy, as well as the first opportunity to study the difference $s(x) - s(x)$. Neutrino induced dimuon production, ($=$) $N \rightarrow \mu^+ \mu^- X$, proceeds primarily through the subprocesses $W^+ s \rightarrow c$ and $W^- s \rightarrow \bar{c}$ respectively, and hence provides independent information on s and s .

We present the first global QCD analysis that includes this new dimuon data. The new results demonstrate, first of all, that the strangeness asymmetry, as measured by the momentum integral $[S] = \int_0^1 x [s(x) - s(x)] dx$, is indeed more sensitive to the dimuon data than to the DIS data, due to an important interplay between the enhanced experimental constraints and the strong theoretical requirements of PQCD. We then use the recently developed Lagrange method of global analysis to explore the range of uncertainty of $[S]$ in the global analysis context. In this first report, we concentrate on $[S]$, the integrated strangeness asymmetry, which represents a new parton degree of freedom in the nucleon heretofore largely unexplored, and which has immediate impact on precision electroweak physics because of the NuTeV anomaly.[2] The full exploration of the density functions $s(x)$ and $s(x)$ will be presented later.

We begin by describing the general features of the strangeness sector of the nucleon structure in the QCD framework, and our general parametrization of that sector. This is followed by the main results of the global analysis, with emphasis on concrete representative global fits relevant for probing the strangeness asymmetry. The paper concludes with a summary of the extensive studies performed beyond the examples given, comparisons to

^aA preliminary version of this study was reported at the Lepton Photon 2003 International Symposium, Fermilab, August 2003. Cf. P. Gambino (arXiv:hep-ph/0311257) and R. Thome (hep-ph/0309343), to be published in the Proceedings.

^bThe strangeness content of the nucleon, as measured by the momentum fraction carried by s or \bar{s} , is of order 3% at $Q = 1.5$ GeV.

previous work on strangeness asymmetry, and conclusions.

2 General properties of $s(x)$ $s(x)$ and its first two moments

For each Q ; let us define the strangeness number densities $s^-(x)$ and their integrals $[s^-]$ by

$$[s^-] = \int_0^{Z_1} s^-(x) dx = \int_0^{Z_1} [s(x) - s^-(x)] dx; \quad (1)$$

and the momentum densities $S^+(x)$ and integrals $[S^+]$ by

$$[S^+] = \int_0^{Z_1} S^+(x) dx = \int_0^{Z_1} x [s(x) - s^-(x)] dx; \quad (2)$$

In the QCD parton model, certain features of these quantities are necessary:

1. The parton distributions $s(x)$ and $s^-(x)$ (or equivalently $s^+(x)$), are parameterized at some low (non-perturbative) scale Q_0 ; the full Q -dependence is then determined by DGLAP evolution.
2. The strangeness number sum rule for the nucleon requires

$$[s^-] = 0 \quad (\text{for all } Q); \quad (3)$$

A necessary corollary is that the density function $s^-(x)$ must be less singular than $1/x$ as $x \rightarrow 0$ for all Q .

3. The momentum sum rule requires

$$[S^+] = 1 - \alpha_0 \quad (\text{for all } Q); \quad (4)$$

where α_0 represents the momentum fraction of all non-strange partons. This condition constrains $[S^+]$ because α_0 is rather well determined by total inclusive DIS and other experiments.

4. In the limit $x \rightarrow 0$ (high energy and fixed Q), Regge considerations and the Pomeranchuk theorem predict $s^-(x) = s^+(x) \rightarrow 0$.

From these general constraints, we draw the following conclusions:

The number sum rule, Eq. (3), implies that a graph of $s^-(x)$ must cross the x -axis at least once in the interval $[0;1]$; and the areas bounded by the curve above and below the x -axis must be equal.

Assuming a simple scenario in which there is only one zero crossing, either $s^-(x) < 0$ in the low x region and $s^-(x) > 0$ in the high x region, or vice versa. The two possibilities imply $[S^-] > 0$ or $[S^-] < 0$, respectively, because the momentum integral suppresses the small x region and enhances the large x region.

According to the parametrizations of $s(x)$ and $s(x)$ used by the CCFR-NuTeV dimuon study [1, 7], $s(x)$ is negative in the x range covered by the experiment ($0.01 < x < 0.3$).^c A previous detailed global analysis of inclusive data by Barone et al. [3] (henceforth referred to as BPZ), finds that $s(x)$ is positive in the large x region. These previous results are shown in Fig. 1 as the two solid curves. When combined with the theoretical constraints

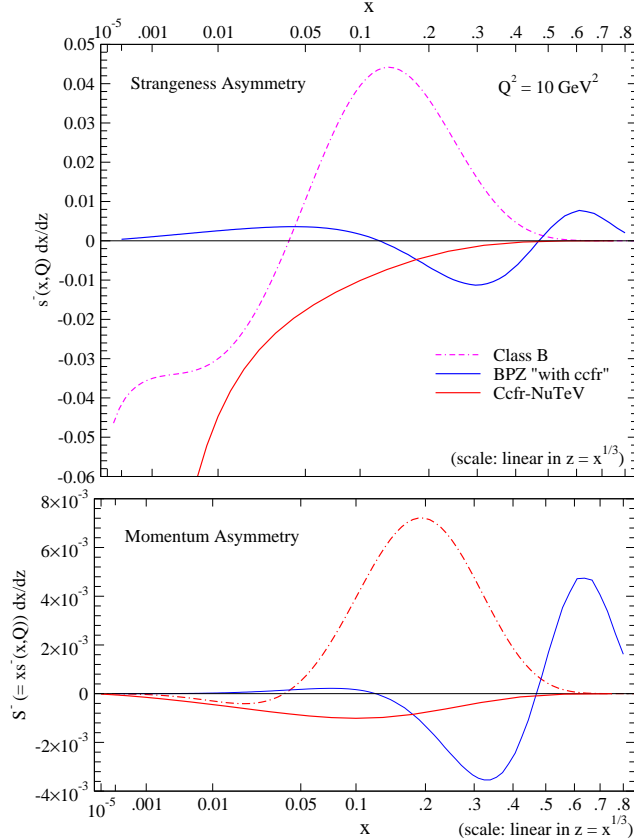


Figure 1: Comparison of $s(x)$ and $S(x)$ for our central $t\backslash B$ (dot-dashed) with those of BPZ and CCFR-NuTeV (solid). The horizontal axis is linear in $z = x^{1/3}$ so that both large and small x regions are adequately represented; the functions are multiplied by a Jacobian factor $dx = dz$ so that the area under the curve is the corresponding integral over x .

discussed above, both these results favor the first possibility mentioned above, i.e. $[S] > 0$. The dash-dotted curves in the two plots of Fig. 1, taken from a representative global fit to be discussed in Sec. 4, provide a concrete example (of $s(x)$ and $S(x)$) that embodies the general features just discussed. The magnitude of $[S]$ will depend on the crossing point and the precise shape of the $s(x)$ curve.

^cSince the preliminary version of this work was reported, the CCFR-NuTeV collaboration has emphasized that their most recent analysis more favors zero strangeness asymmetry (K. M. MacFarland and P. Spentzouris, communications at the LP03 Symposium and WIN03 Workshop). More definitive studies are needed to clarify the situation. See further discussions in Sec. 5.

Because the experimental constraints are weak or non-existent in the very small x region, say $x < 0.01$, the detailed behavior of $s^-(x)$ is unconstrained in this region, as shown by the various classes of solutions displayed in the upper plot of Fig. 2 (taken from fits to be discussed in Sec. 4). However, this uncertainty at small x has little consequence for $S^-(x)$, as explicitly demonstrated by the curves of the lower plot. Thus the above observations concerning $[S^-]$ are not much affected by the uncertainty of the very small x behavior, unless that behavior is so extreme that the small x region provides a significant contribution to the number sum rule.

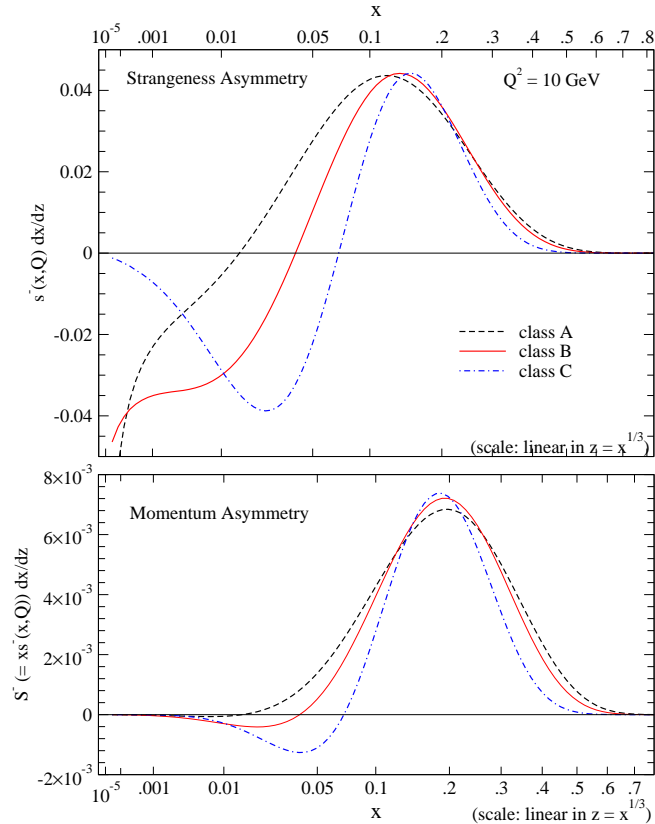


Figure 2: Typical strangeness asymmetry $s^-(x)$ and the associated momentum asymmetry $S^-(x)$, as obtained in our global analysis. The axes are the same as in Fig. 1.

3 General parametrization of the strangeness distributions

To explore the strangeness sector of the parton structure of the nucleon, we need a suitable parametrization of $s^-(x)$ and $s^+(x)$ (or equivalently $s^-(x)$) at a fixed scale Q_0 . This parametrization must satisfy the theoretical requirements specified above, and it should be as general as possible so that the allowed functional space can be fully explored. A general

parametric form is essential, so that our conclusions are not artifacts of the parametrization, but truly reflect the experimental and theoretical constraints.

It is more natural to parametrize the $s^+(x;Q_0)$ functions independently (rather than s and s^+) since they satisfy different QCD evolution equations: pure non-singlet for s^+ and mixed singlet/non-singlet for s . We use the following parametrizations,

$$s^+(x;Q_0) = A_0 x^{A_1} (1-x)^{A_2} P_+(x;A_3;A_4;\dots) \quad (5)$$

$$s(x;Q_0) = s^+(x;Q_0) \tanh[a x^b (1-x)^c P^-(x;x_0;d;e;\dots)] \quad (6)$$

where $P_+(x;A_3;\dots)$ is a positive definite, smooth function in the interval $(0;1)$, depending on additional parameters $A_3;\dots$ such as are used for $u;d;g;\dots$ in most CTEQ [8] and other global analyses [9,10]; and

$$P^-(x) = 1 - \frac{x}{x_0} - 1 + dx + ex^2 + \dots \quad (7)$$

where the crossing point x_0 is determined by the strangeness number sum rule $[s] = 0$, and the parameters $d;e;\dots$ are optional, depending on how much detail is accessible with the existing constraints. Important features of this parametrization are the following:

The strangeness quantum number sum rule, $[s] = 0$, is satisfied by the choice of x_0 . The parameter x_0 has a physical interpretation: it is the "crossing point" where $s(x) = 0$. (If d and/or e are not zero, there can be additional zeros of $s(x)$.)

The fact that the tanh function has absolute value less than 1 ensures positivity of $s(x)$ and $s^+(x)$. The fact that tanh is a monotonic function guarantees that the function $s(x)$ can be made as general as necessary by the choice of $P^-(x)$.

The small- x behavior of $s(x)$ must be such that the integral $[s]$ converges (before the root x_0 is determined). Let $A_1 + b$; then Eq. (6) implies

$$s(x) \propto x \quad \text{as } x \rightarrow 0: \quad (8)$$

The convergence of $[s]$ is guaranteed if $b > -1$, i.e. the parameter b is chosen in the range $b > -1 - A_1$.

Because $P^-(x)$ can be made as general as necessary, the choice in Eqs. (5) { (7) is capable of exploring the full strangeness parameter space allowed by data in the PQCD framework.

4 Global Analysis

We now describe the global QCD analysis, which includes all relevant experimental data and implements the theoretical ideas outlined above. This may be considered an extension of the on-going CTEQ program of global analysis. Several new elements (compared to the latest CTEQ 6M [8] and CTEQ 6HQ [11] analyses) are present. On the experimental side, we have added the CDHSW inclusive F_2 and F_3 data sets [12], the CCFR-NuTeV dimuon data sets

[1] and the new E866 pp Drell-Yan data set [13]. On the theoretical side, we have expanded the parameter space to include the strangeness sector as discussed in Sec. 3.

Compared to the global analyses of BPZ [3], which have also allowed $s \neq s$, the major difference experimentally is our inclusion of the dimuon data, which provide a direct handle on s and s ; and, theoretically, the generality and naturalness of our parametrization of the strange distributions.^d Since the results of [3] on strangeness asymmetry rely on small differences of inclusive D IS charged-current and neutral-current measurements, BPZ took great pains in performing the analysis at the cross section level, applying uniform procedures to treat data from different experiments in the comparison to theory. Now that the dimuon data are available to constrain the strange distributions, such an elaborate procedure offers very limited advantage; furthermore, the differences are intrinsically uncertain. Therefore, for all inclusive D IS processes we use the standard procedure of comparing theory with the published F_2 and F_3 structure function data. In our analysis, the t to charged-current (neutrino) inclusive structure functions is dominated by the high statistics CCFR data. Although we have included the earlier inclusive CDHSW data (which play a prominent role in the analysis of [3]), they have no discernible influence on the results presented below.

To include the CCFR-NuTeV neutrino and antineutrino dimuon production data in a global QCD analysis is not a straightforward task. The experimental measurement is presented as a series of "forward differential cross sections" with kinematic cuts, whereas the theoretical quantities that are most directly related to the parton distribution analysis are the underlying "charm quark production cross sections." The gap between the two is bridged using a Monte Carlo program that incorporates kinematic cuts as well as fragmentation and decay models. In our analysis, we use a Pythia program provided by the CCFR-NuTeV collaboration.^e This Monte Carlo calculation is done in the spirit and the framework of leading-order (LO) QCD. CTEQ 5L parton distributions and Peterson fragmentation functions were used. The parameters of the model were tuned to reproduce, as closely as possible, the detailed differential dimuon cross sections published in [1]. Because the only available data sets are converted by this procedure, we use LO theoretical formulas for the charm cross section in the current analysis. Our results show that the uncertainties resulting from existing experimental constraints are quite large, so the LO treatment is adequate for this first study of the dimuon data in a global QCD analysis context. All fully inclusive (large) cross sections used in this global analysis are treated in NLO QCD; the precision of these data sets demands that level of accuracy. Using an LO approximation for the dimuon data in this NLO analysis is not ideal; however, within current experimental uncertainties, the NLO corrections to the charm production cross section are not large enough to affect the qualitative features of our analysis. In Sec. 4.4, we will discuss the robustness of our results. We will also briefly describe a series of purely LO fits, which are carried out for comparison

^dRef. [3] parametrizes $s(x)$ and $s(x)$ in simple form s , rather than $s(x)$. We prefer to parametrize $s(x)$ for the reasons given in Sec. 3.

^eWe thank Tim Bolton and Max Goncharov, in particular, for providing this program, as well as assistance in its use. Their help was vital for carrying out this project.

purposes. (The existing experimental analysis [1] was done in LO.)

4.1 Procedure

Our analysis is carried out in several stages.

1. We first fix all of the "conventional" parton parameters to their values in the CTEQ 6M parton distribution set, and fit the complete set of data by varying only the parameters associated with the new degrees of freedom in s . We observe that: (i) most of the data sets used in the previous analysis are not affected at all by the variation in s (as they should not be); (ii) a few fully inclusive cross sections are slightly affected by the variation of s (such as F_3 which depends on $u + d + s$::), but the sensitivities are weak; and (iii) the CCFR-NuTeV dimuon data sets are the most constraining ones for fitting s . We obtain good fits using either the 3-parameter ($a; b; c$) or the 4- or 5-parameter ($a; b; c; d; e$) versions of Eqs.(6,7). There is not enough constraint to choose among these. The higher-order polynomials allow oscillatory behavior of $s(x)$ which the 3-parameter form does not.
2. Using these candidate fits as a basis, we perform a second round of fitting allowing the parameters associated with s^+ , Eq.(5), to vary in addition to the s ones. This improves the fit to all data sets slightly. We observe that the shape of $s^+(x)$ now deviates from the starting configuration where $s^+(x)$ was set proportional to $u(x) + d(x)$. Defining the strangeness fraction parameter as the ratio of the momentum fraction carried by the strange quarks, $[S^+]$, to that carried by $u + d$ at Q_0 (chosen as $Q_0 = 1.3$ GeV in our study), we find that it may vary in the range 0.3 ± 0.5 ; χ^2 has a shallow minimum around $= 0.4$. This value agrees with previous analyses.

Because the experimental constraints are not sufficient to uniquely determine all the s and s^+ parameters, we categorize several classes of equally good solutions based on such factors as the number of crossing points of $s(x)$, and the behavior of $s(x) = s^+(x)$ as $x \rightarrow 0$ or $x \rightarrow 1$.

3. We finalize these classes of solutions by allowing all parton parameters to vary so that the non-strange parton distributions can adjust themselves to yield the best fit to all the experimental data sets. (As one would expect, these final adjustments are generally small.) The differences in the χ^2 values between the various categories of solutions are not significant.

4.2 Central Results

The following description of results is based on a few representative examples chosen from a large number of candidate fits obtained by the above procedure. The quality of the fits to the global data sets other than the CCFR-NuTeV dimuon data remains quite similar to the previous CTEQ 6M analysis, so we focus our discussion on the strangeness sector. Specifically, we examine closely the asymmetry functions $s(x)$; $S(x)$ and the momentum integral $[S]$. The asymmetry functions from three typical good fits, with different behaviors at small x (labeled as classes A, B, C), were previewed in Fig.2 as illustrations.

In the accompanying table, for each sample we list the small- x exponent $s(x)$, the integrated momentum fraction $[S]$, and the relative χ^2 values, normalized to the χ^2 of solution B, which we use as the reference for comparison purposes. (Under column 'B', we give the absolute χ^2 's in parentheses.)^f To gain some insight on the constraints on the strangeness sector due to the various types of experiments, we show separately the χ^2 values for the dimuon data sets, the inclusive data sets (I) that are expected to be somewhat sensitive to s (consisting of the CCFR and CDHSW $F_3(x;Q)$) and the CDF W -lepton asymmetry measurements), and the remaining ones (II) that are only indirectly affected by s (the rest of the inclusive data sets).

	# pts	B+	A	B	C	B
	-	0.78	0.99	0.78	0	0.78
$[S]$	100	-	0.540	0.312	0.160	0.103
Dimuon	174	1.30	1.02	1.00 (126)	1.01	1.26
Inclusive I	194	0.98	0.97	1.00 (141)	1.03	1.09
Inclusive II	2097	1.00	1.00	1.00 (2349)	1.00	1.00

Table 1. Features of the representative parton distribution sets described in the text, arranged by the order of the value of $[S]$ from left to right.

Focusing on the three good fits f_A, f_B, f_C first, we note the following.

All three solutions f_A, f_B, f_C feature positive $[S]$; and the more singular the behavior of $s(x)$ as $x \rightarrow 0$, the higher the value of $[S]$. These are natural consequences of the strangeness sum rule (equal $\int s(x) dx$ = areas under the curve of $s(x)$) and the small- x suppression of the momentum integral, as discussed earlier in Sec. 2.

Solution B is slightly favored over the other two. This, plus the fact that its small- x behavior lies in the middle of the favored range, motivates its use as the reference fit.

We chose these examples among fits with the simplest parametrizations: all cross the x axis only once. With 4- or 5-parameters, which can allow more than one crossing point, many solutions can be found that entail oscillatory $s(x)$. But since the χ^2 values are substantially the same as for the simple case, we deem it premature to dwell on complicated behaviors, which may be mere artifacts of the parametrization rather than reactions of physical constraints. Further studies described in Sec. 4.4 reinforce this point.

To show how these fits compare with data, we plot in Fig. 3 the ratio of data/theory for the reference fit B. The four graphs correspond to the CCFR and NuTeV neutrino and antineutrino data sets respectively. The data points are sorted in x -bins, and within each

^fThe χ^2 values of the dimuon data sets, like those of some other data sets, do not carry rigorous statistical significance, because the correlated systematic errors are not available and, hence, cannot be included. In the global analysis context, the χ^2 value is nevertheless used as the only practical "figure of merit" for the fit. The relatively small value of the total χ^2 for the dimuon data sets, compared to the number of data points, underlines this fact. Under this circumstance, it is common practice to use the normalized χ^2 values to compare the quality of different fits.

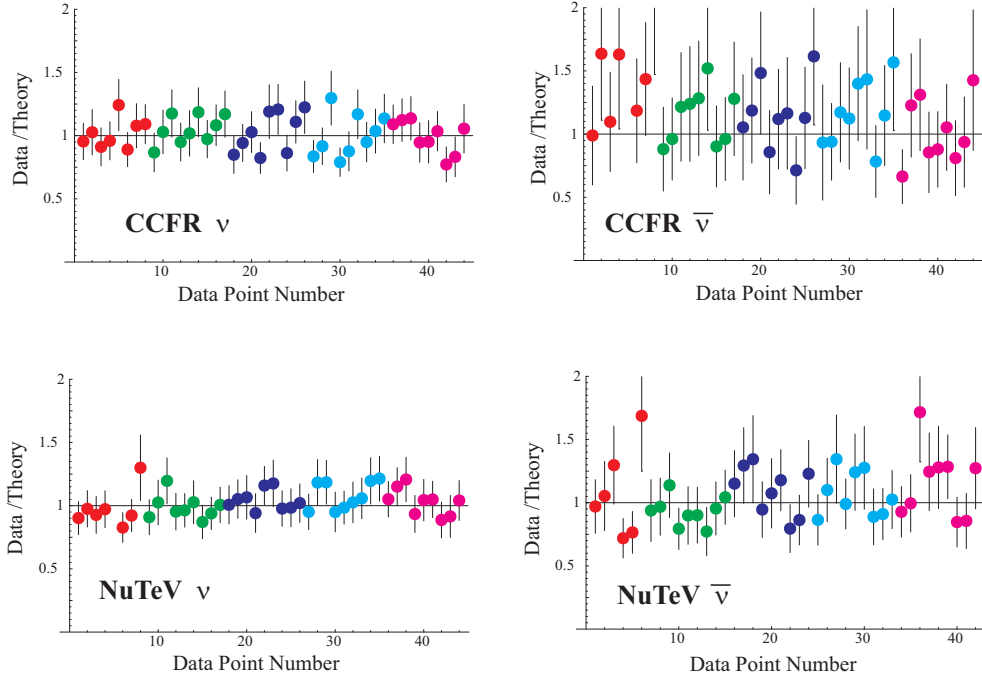


Figure 3: Comparison of data to tB .

x-bin, by y value. We see that the quality of the t is good, within the experimental uncertainties. There are no significant systematic deviations. (The CCFR antineutrino data set may appear to be systematically higher than theory. However, upon closer inspection the difference is not significant. The data points that lie above theory consist mostly of points with large error bars, which tend to catch the attention of the eye; whereas the t is actually dominated by points with small errors, which closely bracket the theory line on both sides.⁹ The value of χ^2/N for this data set is less than 1, comparable to those for the other sets.)

4.3 Range of $[S]$ by the Lagrange Multiplier Method

Beyond the best ts (A, B, C), we can study the range of $[S]$ consistent with our global analysis in a quantitative way by applying the Lagrange Multiplier (LM) method developed in [14]. By varying the Lagrange multiplier parameter, this method explores the entire strangeness parameter space in search of solutions with specified values of $[S]$, i.e., constrained ts . The B^- solution listed in Table 1 was obtained by forcing $[S] = -0.0018$ (a relatively large negative value, but not as large as the value -0.0027 cited by [5,7]). The B^+ solution was generated by forcing $[S]$ to go in the other (positive) direction until the increment of the overall χ^2 became comparable to that of B^- ; this results in $[S] = 0.0054$.

We see from the relevant entries in Table 1 that: (i) the χ^2 values of the dimuon data sets increase by about 30% in both B ts ; (ii) the “inclusive I” data sets disfavor the negative $[S]$; and (iii) the “inclusive II” data sets are completely neutral. These results

⁹This becomes apparent if the data points are re-plotted ordered by the size of the error bars.

are shown graphically in Fig. 4, where the square points represent the (relative) χ^2 values of the dimuon data sets, and the triangle points of the “inclusive I” data sets. (Not shown are those for the “inclusive II” data sets, which remain at (at 1:00).) The LMs fits are chosen from a large number of fits spanning the entire strangeness parameter space. The pattern of dependence of the χ^2 values for the dimuon data sets on the value of $|S_-|$ is nearly parabolic. This is clear evidence that the dimuon measurement is indeed sensitive to the strangeness asymmetry as expected. Further discussion of this observation, including the contrast to the sensitivity of other experiments, will be given in Sec. 4.4.

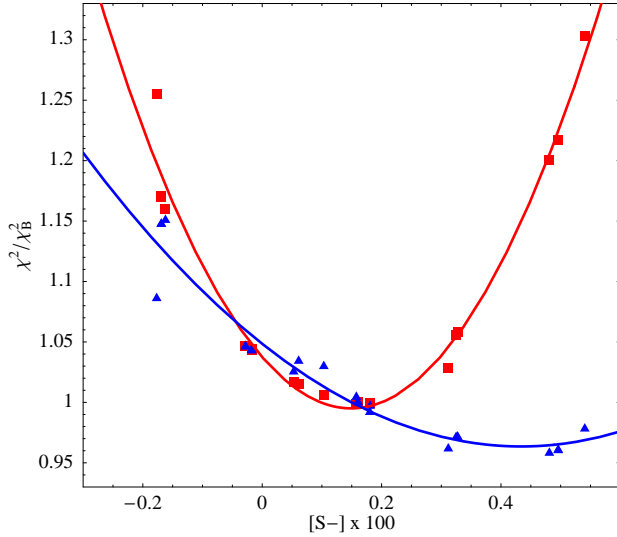


Figure 4: Correlation between χ^2 values and $|S_-|$.

We see from Fig. 4 that, in this series of fits, the dimuon data sets favor a range of $|S_-|$ centered around 0.0017, whereas the “inclusive I” data sets disfavor negative values of $|S_-|$. Taken together, a reasonable allowed range for $|S_-|$ might be estimated to be 0.001 { 0.003, although a value of zero (no strangeness asymmetry) is not necessarily ruled out. Large negative values of $|S_-|$ are clearly disfavored; cf. also Table 1.

The parton distribution functions associated with the sample sets listed in Table 1 will be available on the CTEQ web page (<http://cteq.org>).

4.4 Additional Sources of Uncertainties

The most obvious weak link of the current analysis is that the comparison of neutrino dimuon data to QCD theory of charm production still depends on a LO model calculation of the fragmentation and decay processes. This weak point should be remedied in the next round of more refined analysis. For the current work, we have performed three series of studies to assess the reliability of our main results.

Pure Leading Order Fits Since the experimental analyses of the CCFR+NuTeV dimuon data have been done in LO QCD [1, 7], we have carried out a whole series of purely LO

global analyses, following the same procedures as outline above, in order to provide a basis for comparison. The results can be summarized as follows.

The overall χ^2 for the global t increased by 200 over the comparable t s described above; while the χ^2 s for the dimuon data sets actually decreased slightly. This is not surprising, since the current state of global analysis, with precision data from many experiments, requires the use of NLO QCD theory. On the other hand, the new dimuon data still have comparably large experimental errors, such that an LO t is adequate for them.

We explored the allowed range of strangeness asymmetry $[S]$ in this LO study under different assumptions on the $x \neq 0$ and $x \neq 1$ behavior of the $s^+(x)$ and $s^-(x)$ functions. First, we found that the χ^2_{dimuon} vs. $[S]$ curves are again close to parabolic, and are rather similar to that of Fig. 4. The widths of the parabolas are comparable to that of Fig. 4; the center of the parabolas wanders within the range $0 < [S] < 0.0015$.

We also found that the $\chi^2_{\text{inclusive}}$ vs. $[S]$ curves, while generallyatter, do "lop around" enough so that no clear pattern can be discerned. The specific shape of this curve shown in Fig. 3 is not a common characteristic of these t s.

Charm Mass Dependence The CCFR-NuTeV dimuon analysis treated the charm mass as one of the t parameters. Their analyses favored a rather high value of $m_c = 1.6$ GeV (compared to, e.g., the PDG estimate of 1.0 GeV $< m_c < 1.4$ GeV). The CTEQ global analyses are usually done with a fixed value of $m_c = 1.3$ GeV. To see whether the comparison between our results is strongly influenced by the choice of the charm mass, we have performed several series of t s with m_c varying from 1.3 GeV to 1.7 GeV. Again, the general features, as described above, stay the same. The central value of $[S]$ does vary with the choice of m_c within a given series of t s, but the pattern is not universal. The range over which the central value wanders is of the order 0.0015, comparable to the width of the parabola in Fig. 4. Unlike the specific analysis of CCFR-NuTeV, the overall χ^2 for the global analysis does favor a lower value of m_c .

Dependence on Decay and Fragmentation Model To estimate the dependence of our results on the model used to convert the measured dimuon cross sections to structure functions for charm production, we repeated our analyses using an alternative conversion table provided by the CCFR-NuTeV collaboration.^h This alternative table is based on Buras-Gaemers PDFs used in CCFR-NuTeV analyses with Collins-Soper fragmentation functions. It is similarly tuned to detailed features of the measured dimuon cross sections as that described in Sec. 4.1.ⁱ The results obtained from the alternative t s are, again, similar to those described earlier: the χ^2_{dimuon} vs. $[S]$ parabola has about the same width; and the

^hWe thank Kevin MacFarland for supplying this table.

ⁱHowever, since our CTEQ 6-like PDFs are rather different from the CCFR Buras-Gaemers PDFs, it is not clear how good the approximation is to use this conversion table. That is, the self-consistency of the procedure is not assured.

central values are in the range $0 < [S] < 0.0015$ slightly to the left of that in Fig. 4, but within the estimated range. The $\frac{2}{\text{inclusive}}$ vs. $[S]$ curves are rather flat, with no definite shape.

Taken together, the results of the additional studies described in these three paragraphs lead to several conclusions. (i) The general features described in Secs. 4.2 and 4.3 are robust. (ii) The central value of $[S]$ wanders around within a range that is consistent with the width of the $\frac{2}{\text{dimuon}}$ vs. $[S]$ parabola. (iii) Taking into account these shifts, we believe a realistic estimate of the range of uncertainty of the strangeness asymmetry is

$$0.001 < [S] < 0.004 : \quad (9)$$

This large range reflects both the limit of current experimental constraints and the considerable theoretical uncertainty, as explicitly discussed in the text. The theoretical uncertainties can be reduced in a refined NLO analysis; the results remain to be seen. The limitations on the experimental constraints will remain, until new experiments are done.

5 Comparisons to previous studies

A comprehensive global QCD analysis with emphasis on the strangeness sector has been carried out previously by BPZ [3].^j Without the dimuon data, which are directly sensitive to strangeness, the results of BPZ implicitly rely on small differences between large neutral- and charged-current inclusive cross sections from different experiments. The latest representative $s(x)$ and $S(x)$ functions extracted by BPZ (the more recent solution "with CCFR (inclusive data)") are shown in Fig. 1, along with our reference TB. The main feature of the BPZ curves is a positive bump at rather large x .^k This feature has been attributed to the influence of the CDHSW data, particularly when re-analyzed at the cross section level along with the other DIS experiments. Their conclusion that data favor a positive value of the momentum integral $[S]$ is in general agreement with our detailed study based on the LM method. However, the different shapes of $s(x)$ seen in Fig. 1 clearly underline the difference in inputs: (i) our results are mainly dictated by the CCFR+NuTeV dimuon data (which are not present in the BPZ analysis); (ii) their results rely on a delicate analysis of DIS cross-section data (not matched in our structure function analysis); and (iii) the flexibility of the parametrizations of the non-perturbative input functions can influence the results.

^jAs mentioned in Sec. 4, BPZ work directly with DIS cross sections (instead of structure functions), with detailed attention to systematic errors and other sources of uncertainties.

^kThe original "without CCFR" solution in [3] has an even more pronounced large- x bump and a smaller negative region. A $s(x)$ function of such magnitude at large x appears to be incompatible with the dimuon data, and it would make $s(x)$ and $S(x)$ behave quite differently than the non-strange sea quarks and the gluon, i.e., $(1-x)^p$, with p in the range 5–10.

The CCFR and NuTeV collaborations performed separate and combined analyses of s and $s(x)$, based on their own dimuon and inclusive cross sections. To parameterize the $s(x)$ and $s(x;Q)$ distributions, they chose the model formula

$$\frac{s(x;Q)}{s(x)} = \frac{u(x;Q) + d(x;Q)}{2} \quad (1-x) \quad (1-x) \quad (10)$$

for all $x;Q$, where u , d , s are fitting parameters.

Curves representing the general behavior of the model (10) at $Q^2 = 10 \text{ GeV}^2$, with parameter values (u, d, s) taken from [1], have been shown in Fig. 1 for comparison with the other distributions. While this model might be acceptable for a limited range of x and Q , it leads to serious problems in general: (i) the strangeness number sum rule $[s] = 0$ is badly violated (in fact, the integral $[s]$ diverges unless $s = 0$), as is the momentum sum rule, Eq. 4; (ii) the QCD evolution equation is violated at LO.¹ The first problem can be clearly seen in Fig. 1.^m

It could be argued that, since the experiment only covers a limited range of x , the enforcement of the sum rules is not critical in extracting limited information on $s(x;Q)$ and $s(x)$. If this point is approximately correct, then the CCFR curve in Fig. 1 implies negative $s(x)$ over most of the experimental x range ($0.01 \leq 0.3$).ⁿ The uncertainty is smaller at the lower x end because of better statistics. It is this feature of the data that we invoked in the general discussion of Sec. 2.

To describe the behavior of $s(x)$ over the full x range, the strangeness number sum rule must be enforced. It also provides a powerful theoretical constraint to the data analysis, as demonstrated in Secs. 2 and 4. Functions that fail to satisfy the sum rules or the QCD evolution equations cannot be true candidates for the universal parton distributions of the PQCD formalism that are required to make predictions for other processes.

6 Conclusion

We find several classes of solutions in the strangeness sector that are consistent with all relevant world data used in the global analysis. The dimuon data are vital in constraining the strangeness asymmetry parameters. The constraints provided by other inclusive measurements, labeled as “inclusive I” in the text, are consistent with those provided by dimuon data, although much weaker. The allowed solutions generally prefer the momentum integral

¹These problems have nothing to do with whether LO or NLO QCD formulas are applied to the non-strangeness sector. They remain in the “NLO” CCFR-NuTeV analysis [7,15].

^mRe-analysis of the CCFR-NuTeV data by the experimental group, taking into account these issues, are underway. Initial results from partial implementations of the above-mentioned theoretical constraints were reported by P. Spentzouris at International Workshop on Weak Interactions and Neutrinos 2003 (WIN03), Lake Geneva, October, 2003.

ⁿThis is consistent with the fact that (without the constraint of sum rules) [7] quotes $[s] = 0.0027 \pm 0.0013$.

$\int_{-1}^1 x [s(x) - \bar{s}(x)] dx$ to be positive. This conclusion is quite robust, and it follows from the basic properties of PQCD and from qualitative features of the experimental data. However, the size of this strangeness moment asymmetry is still quite uncertain; we can only estimate that $[S]$ lies in the range from -0.001 to $+0.004$. The Lagrange Multiplier method explicitly demonstrates that both the dimuon data and the "inclusive I" data sets strongly disfavor a large negative value of $[S]$, although they may still be consistent with zero asymmetry.

The fact that $[S]$ has a large uncertainty has significant implications for the precision measurement of the weak mixing angle, $\sin^2 \theta_W$, from neutrino scattering. This issue is studied separately in Ref. [16].

This paper marks the first global QCD analysis incorporating direct experimental constraints on the strangeness sector. We have so far focused only on the strangeness asymmetry, which represents a new frontier in parton degrees of freedom. Much still needs to be done to improve the treatment of the dimuon data (to true NLO accuracy), and to fully explore all the degrees of freedom associated with $s^+(x)$ and $s^-(x)$. As progress is made on these fronts, the uncertainty on $[S]$ will no doubt decrease as well. Results of these further studies will be reported as they become available.

Acknowledgment

We thank members of the CCFR and NuTeV collaboration, in particular T. Bolton and M. Gondcharov, for discussions about the dimuon data, and assistance in their use, and Kevin McFarland and Panagiotis Spentzouris for useful comments and suggestions. We also thank Benjamin Portheault for discussions of the BPZ work and for assistance in generating their results for comparison. F.O. acknowledges the hospitality of MSL and BNL where a portion of this work was performed. This research was supported by the National Science Foundation (grant No. 0100677), RIKEN, Brookhaven National Laboratory, and the U.S. Department of Energy (Contract No. DE-AC02-98CH10886, and No. DE-FG03-95ER40908), and by the Lightner-Samis Foundation.

References

- [1] CCFR and NuTeV Collab. (M. Gondcharov et al.), *Phys. Rev. D* 64, 112006 (2001); NuTeV Collab. (M. Tzanov et al.), *hep-ex/0306035*.
- [2] NuTeV Collaboration, G.P. Zeller et al., *Phys. Rev. Lett.* 88, 091802 (2002).
- [3] V. Barone, C. Pascaud, F. Zomer, *Eur. Phys. J. C* 12, 243 (2000); this analysis is currently being updated and early results have been presented by B. Portheault at DIS03; <http://www.desy.de/dis03>.
- [4] S. Davidson, S. Forte, P. Gambino, N. Rius, A. Strumia, *JHEP* 0202, 037, 2002.

[5] K. S. M. cFarland and S.-O. M och, hep-ph/0306052.

[6] P. G ambino, hep-ph/0211009; A. Strum ia, hep-ex/0304039.

[7] NuTeV Collaboration, G. P. Zeller, Phys. Rev. D 65, 111103 (2002), and D 67, 119902 (2003) (E); K. S. M. cFarland et al., proceedings of 16th Les Rencontres de Physique de la Vallée d'Aoste: Results and Perspectives in Particle Physics, La Thuile, Aosta Valley, Italy, 3-9 Mar 2002, arX iv:hep-ex/0205080.

[8] J. Pumplin, D. R. Stump, J. Huston, H. L. Lai, P. Nadolsky and W. K. Tung, JHEP 0207, 012 (2002).

[9] A. D. Martin, R. G. Roberts, W. J. Stirling, R. S. Thorne, Eur. Phys. J. C 23, 73 (2002).

[10] M. Glück, E. Reya and A. Vogt, Eur. Phys. J. C 5, 461 (1998).

[11] S. Kretzer, H. L. Lai, F. J. O. lnness, and W. K. Tung, hep-ph/0307022.

[12] P. Berge et al., Z. Phys C 49, 187 (1991).

[13] J. C. W ebb et al. [NuSea Collaboration], arX iv:hep-ex/0302019.

[14] J. Pumplin, D. R. Stump, W. K. Tung, et al., Phys. Rev. D 65, 014011 (2002); Phys. Rev. D 65, 014013 (2002); Phys. Rev. D 65, 014012 (2002).

[15] M. Tzanov et al. [NuTeV Collaboration], arX iv:hep-ex/0306035.; to appear in the proceedings of 38th Rencontres de Moriond on QCD and High-Energy Hadronic Interactions, Les Arcs, Savoie, France, 22-29 Mar 2003.

[16] S. Kretzer et al., hep-ph/0312322.